The Astrophysical Journal Supplement Series, 279:53 (10pp), 2025 August https://doi.org/10.3847/1538-4365/ade3ca

A Metallicity Catalog of Very Metal-poor Main-sequence Turn-off and Red Giant Stars from LAMOST DR10

Xiangyu Li[1,2], Huiling Chen[3,4], Yang Huang[1,2,6], Huawei Zhang[3,4,6], Timothy C. Beers[5], Linxuan Zhu[3,4], and Jifeng Liu[1,2]
[1] National Astronomical Observatories, Chinese Academy of Sciences, Beijing 100101, People's Republic of China; huangyang@ucas.ac.cn
[2] School of Astronomy and Space Science, University of Chinese Academy of Sciences, Beijing 100049, People's Republic of China
[3] Department of Astronomy, School of Physics, Peking University, Beijing 100871, People's Republic of China; zhanghw@pku.edu.cn
[4] Kavli Institute for Astronomy and Astrophysics, Peking University, Beijing 100871, People's Republic of China
[5] Department of Physics and Astronomy and JINA Center for the Evolution of the Elements (JINA-CEE), University of Notre Dame, Notre Dame, IN 46556, USA
Received 2025 April 28; revised 2025 June 10; accepted 2025 June 10; published 2025 August 5

Abstract

We present a catalog of 8440 candidate very metal-poor (VMP; [Fe/H] $\leqslant -2.0$) main-sequence turn-off (MSTO) and red giant stars in the Milky Way, identified from low-resolution spectra in LAMOST DR10. More than 7000 of these candidates are brighter than G 16, making them excellent targets for high-resolution spectroscopic follow-up with 4–10 m class telescopes. Unlike most previous studies, we employed an empirical calibration to estimate metallicities from the equivalent widths of the calcium triplet lines, taking advantage of the high signal-to-noise ratio in the red arm of LAMOST spectra. We further refined this calibration to improve its reliability for more distant stars. This method enables robust identification of VMP candidates with metallicities as low as [Fe/H] $= -4.0$ among both MSTO and red giant stars. Comparisons with metal-poor samples from other spectroscopic surveys and high-resolution follow-up observations confirm the accuracy of our estimates, showing a typical median offset of 0.1 dex and a standard deviation of 0.2 dex.

Unified Astronomy Thesaurus concepts: Chemical abundances (224); Galaxy stellar content (621); Halo stars (699); Population II stars (1284)

Materials only available in the online version of record: machine-readable table

1. Introduction

Very metal-poor (VMP; [Fe/H] $\leqslant -2.0$) stars serve as fossil records of the early chemical enrichment and dynamical assembly of the Milky Way. Their chemical compositions offer valuable clues about the star formation history of the early Universe, as well as the nature of the Big Bang, the initial mass function, the nucleosynthetic yields of the first generations of stars, and the role of early supernovae in shaping the interstellar medium (T. C. Beers & N. Christlieb 2005; M. N. Ishigaki et al. 2018; R. S. Klessen & S. C. O. Glover 2023). In addition, the dynamical properties of VMP stars provide key insights into the formation of the Galactic halo and the major merger events that occurred during the Galaxy's early assembly history (e.g., D. Shank et al. 2022, 2023; J. Zepeda et al. 2023; J. Cabrera Garcia et al. 2024, and references therein).

Due to their rarity and scientific significance, the search for VMP stars has long been a challenging yet central pursuit in Galactic archeology. Over the past decade, large-scale spectroscopic and photometric surveys have enabled unprecedented opportunities for their discovery. Millions of VMP candidates have been identified through data mining of spectroscopic surveys such as RAVE (M. Steinmetz et al. 2006), LAMOST (X.-Q. Cui et al. 2012; G. Zhao et al. 2012), SEGUE (B. Yanny et al. 2009; C. M. Rockosi et al. 2022), APOGEE (S. R. Majewski et al. 2017), GALAH (G. M. De Silva et al. 2015), and Gaia (Gaia Collaboration et al. 2023), objective-prism surveys such as the HK survey (T. C. Beers et al. 1985, 1992) and the Hamburg/ESO survey (N. Christlieb et al. 2008), and photometric surveys like the Pristine survey (E. Starkenburg et al. 2017), the SkyMapper survey (C. Wolf et al. 2018; Y. Huang et al. 2019, 2022), J-PLUS (A. J. Cenarro et al. 2019; Y. Huang et al. 2024), S-PLUS (C. Mendes de Oliveira et al. 2019, Y. Huang et al. 2025, in preparation), and SAGES (Z. Fan et al. 2023; Y. Huang et al. 2023). However, many of these samples are based on survey pipelines or machine learning methods, which generally struggle to identify stars below [Fe/H] -2.5 due to the intrinsic weakness of metal lines at such low abundances. In the case of the photometric surveys, the influence of strong molecular carbon bands can lead to incorrect (high) metallicity estimates (see, e.g., J. Hong et al. 2024).

Although high-resolution spectroscopic follow-up provides precise measurements, the number of VMP stars confirmed through such observations remains relatively small. A major limitation lies in the low success rate of candidate selection from low-resolution or photometric data—many turn out not to be truly metal poor. This leads to a significant waste of valuable high-resolution resources and hinders the construction of reliable VMP samples. These challenges underscore the urgent need for a large and reliable sample of VMP candidates that can efficiently guide follow-up efforts toward the most promising targets.

LAMOST DR10 has released over 12 million low-resolution stellar spectra across the Milky Way, offering a rich data set for stellar parameter and chemical-abundance analysis. With its wide wavelength coverage (3700–9100 Å)

[6] Corresponding authors.

and sufficient spectral resolution (R 1800), LAMOST enables the determination of multiple elemental abundances and atmospheric parameters (G. Zhao et al. 2012). Most existing pipelines, such as those described in A. L. Luo et al. (2015) and H. Li et al. (2018), primarily focus on the blue arm of the spectrum, where metal absorption lines are abundant. However, for VMP stars, the blue spectral region often suffers from low signal-to-noise ratios (SNR), making metallicity measurements challenging due to the intrinsic weakness of metal lines, and/or poor determination of the continuum. In contrast, the red arm of LAMOST spectra typically exhibits significantly higher SNR, which is crucial for detecting and characterizing distant and faint VMP stars. Fully leveraging this high-SNR red spectral range allows for the identification of a larger number of reliable VMP candidates than previously possible, and improves the precision of metallicity estimates for already known ones.

Since the red arm of LAMOST spectra contains fewer spectral features than the blue arm, we abandoned the synthetic spectral-fitting methods commonly adopted by LAMOST pipelines and employ an alternative approach. We focus on the calcium triplet (CaT) lines (λ = 8500, 8544, 8664 Å), which are among the most prominent features in the near-infrared region of LAMOST spectra. R. Carrera et al. (2013) demonstrated that the CaT lines serve as reliable metallicity indicators for VMP red giant stars, and provided a simple empirical calibration capable of measuring metallicities down to [Fe/H] −4.0 using their equivalent widths (EWs). A. Viswanathan et al. (2024) further applied this method to Gaia Radial Velocity Spectrometer (RVS) spectra, showing excellent agreement with high-resolution spectroscopic measurements, confirming its robustness.

Building on these studies, we adopt the empirical calibration of R. Carrera et al. (2013) to estimate metallicities for red giant stars in our sample. Calibrated on VMP red giants in globular clusters with non–local thermodynamic equilibrium effects considered, this method is well suited for red giants. We also test its performance on other stellar types, and find that it yields reliable metallicities for MSTO stars, though it is not applicable to dwarf or blue giant stars. Applied to LAMOST spectra, this method enables the identification of a large number of candidate VMP MSTO and red giant stars with robust metallicity estimates.

Using this method, we present a catalog of 8440 VMP candidates selected from LAMOST DR10, along with their estimated metallicities. Section 2 describes the data set used in this study. Section 3 outlines the candidate selection and metallicity-estimation procedures. In Section 4, we present the metallicity results and evaluate their reliability through comparisons with high-resolution spectroscopic samples, other spectroscopic surveys, and machine learning–based estimates. Section 5 summarizes our findings and discusses the potential of this approach for future studies.

2. Data

In this study, we primarily utilize spectroscopic data from LAMOST DR10 (X.-Q. Cui et al. 2012) and photometric and astrometric data from Gaia DR3 (Gaia Collaboration et al. 2023). LAMOST currently has the world's largest (ground-based) stellar spectral database, and its latest public release, DR10, provides over 12 million stellar spectra in the Milky Way. With its wide wavelength coverage (3700–9100 Å), LAMOST enables robust determination of stellar parameters and elemental abundances.

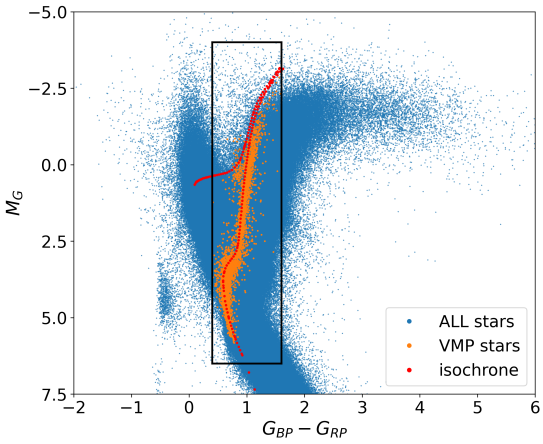

Figure 1. Color–magnitude diagram of stars in LAMOST DR10. The black rectangle indicates our empirical cut for MSTO and red giant stars, defined by $0.4 < G_{\rm BP} - G_{\rm RP} < 1.6$ and $-4.0 < M_G < 6.5$. The blue data points represent the full stellar sample from LAMOST DR10, while the orange data points represent the VMP stars identified by Method 1. These stars exhibit a good agreement with the PARSEC isochrone for [Fe/H] = −2.0 and an age of 10 Gyr, shown as the red-dotted line.

Table 1
Coefficients for the Calibrations Used in This Work

Coefficients	Method 1		Method 2	
a	−3.45	0.04	−3.68	0.15
b	0.16	0.01	−0.72	0.12
c	0.41	0.004	0.49	0.01
d	−0.53	0.11	0.35	0.02
e	0.019	0.002	...	

Note. Coefficients in Method 1 are taken from R. Carrera et al. (2013).

To ensure data quality, we selected low-resolution LAMOST spectra with SNR greater than 20 in the r band, which ensures reliable measurements, particularly in the near-infrared. For stars with multiple observations, we retained the spectrum with the highest SNR. These were then crossmatched with Gaia DR3 sources to incorporate magnitudes and distances, adopting the geometric distance estimates from C. A. L. Bailer-Jones et al. (2021).

3. Methods

3.1. Method 1: The Absolute Magnitude Method

The absolute magnitude method (hereafter referred to as Method 1) is based on the calibration provided by R. Carrera et al. (2013), which requires CaT EWs and absolute magnitudes as inputs, as expressed in Equation (1). We found that R. Carrera et al. (2013) offered four sets of coefficients for different photometric systems, and the results obtained using these four coefficient sets all showed good consistency. Therefore, we chose the coefficient set using Johnson–Cousins V magnitudes as input. Some of the candidates did not have precise V magnitudes, so we used the conversion provided by M. Riello et al. (2021) to convert Gaia G magnitudes to V magnitudes. The coefficients are shown in the left column

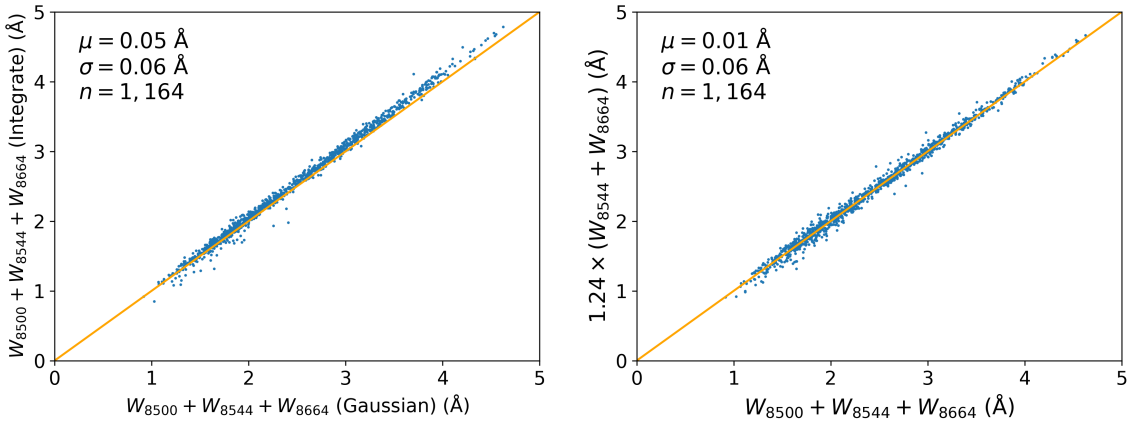

Figure 2. Left: comparison of the sum of the EWs of three CaT lines, $W_{8500} + W_{8544} + W_{8664}$, for the high-SNR VMP sample using the Gaussian-fitting method and direct integration method. Right: comparison of two definitions of ΣCa: the sum of the three lines $W_{8500} + W_{8544} + W_{8664}$, and 1.24 times the sum of the last two lines $1.24 \times (W_{8544} + W_{8664})$. The number of samples (n), median offset (μ), and standard deviation (σ) are shown at the top. The orange line represents the 1:1 line.

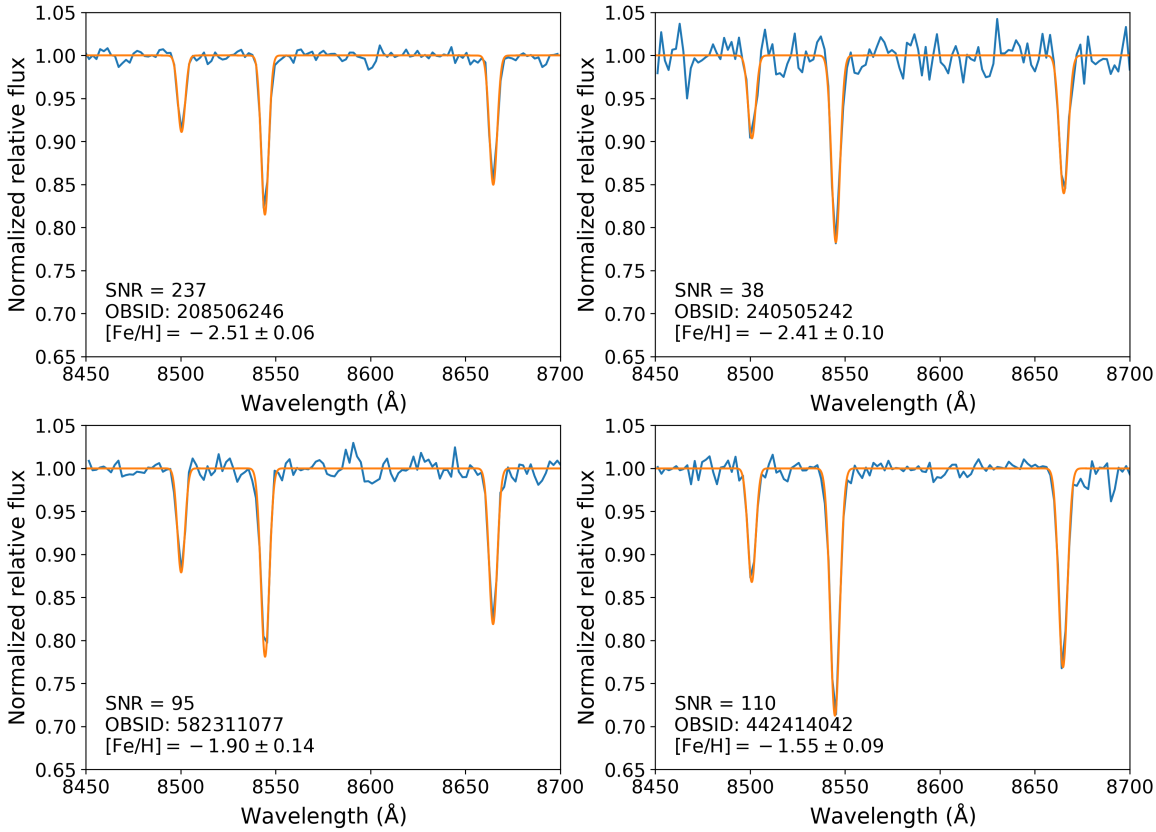

Figure 3. Normalized spectra and fitted CaT lines for four example stars in this work. OBSID stands for LAMOST DR10 unique spectrum ID. These examples cover the main range of metallicities and SNRs of our samples. The blue line represents the normalized spectra, and the orange line represents the fitted CaT lines.

of Table 1.

$$[\mathrm{Fe/H}] = a + b \times M_V + c \times \Sigma\mathrm{Ca} + d \times \Sigma\mathrm{Ca}^{-1.5} + e \times \Sigma\mathrm{Ca} \times M_V. \quad (1)$$

3.1.1. Candidate Selection

The calibration from R. Carrera et al. (2013) is intended for red giant stars, but we also tested its performance on other stellar types and compared the results with metal-poor samples from high-resolution spectroscopy. We find that this calibration yields reliable metallicities for MSTO stars with absolute magnitudes brighter than G 6.5, though it is not applicable to dwarf or blue giant stars. Thus, we adopt an empirical cut from Y. Huang et al. (2022) based on Gaia G magnitudes and Gaia BP − RP color: $0.4 < G_{\mathrm{BP}} - G_{\mathrm{RP}} < 1.6$ and $-4.0 < M_G < 6.5$, to select MSTO and red giant stars. The cut is shown as the black rectangle on the color–magnitude diagram in Figure 1. We then crossmatched the selected

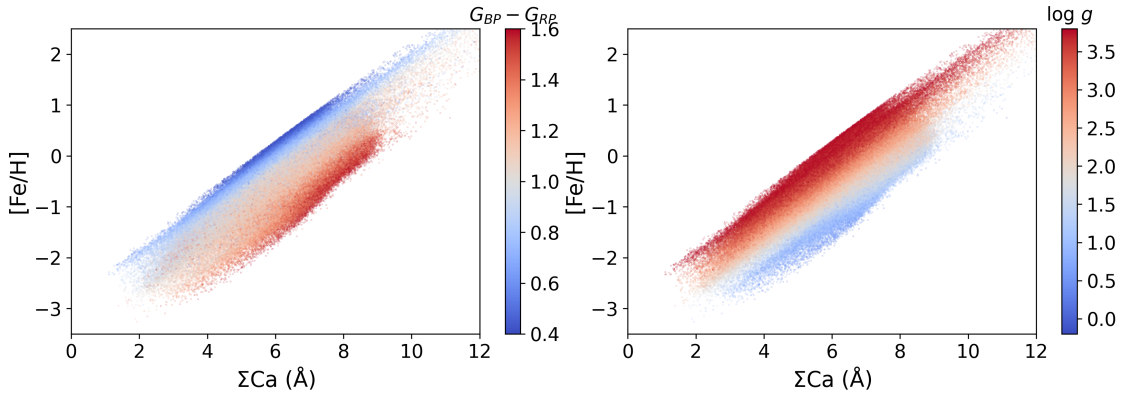

Figure 4. The correlation between metallicity and the CaT index, Gaia BP − RP color (left), and surface gravity (right). The metallicities are estimated by Method 1, while the surface gravity values are estimated by LASP. This color map shows that metallicity has a strong relationship with the CaT index, Gaia BP − RP color, and surface gravity.

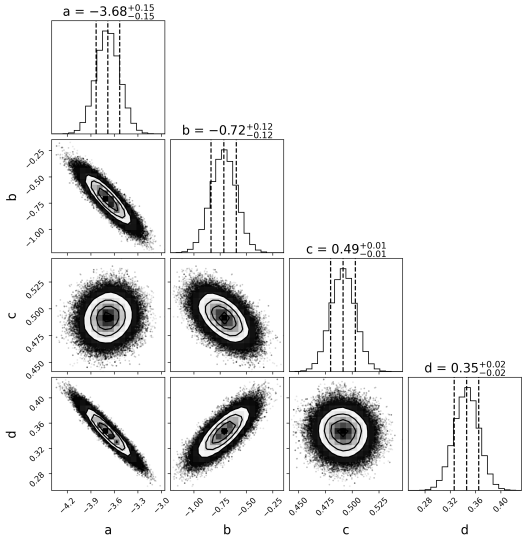

Figure 5. The MCMC result for the coefficients in Equation (2). The values at the top of the columns represent the median offset and 1σ standard deviation of the coefficients. This figure shows good fitting results, indicating that the coefficients are reliable.

MSTO and red giant stars with the LAMOST stellar parameter catalog, derived from LAMOST low-resolution spectra using the LAMOST stellar parameter pipeline (LASP; A. L. Luo et al. 2015). This catalog presents metallicities for stars in LAMOST DR10 with a selection criterion of [Fe/H] > -2.5. We further exclude stars with [Fe/H] > -1.5, as they are unlikely to be VMP stars. The final sample comprises approximately 200,000 MSTO and red giant stars with [Fe/H] < -1.5.

3.1.2. Spectral Metallicity Estimate Pipeline

First, we shifted all LAMOST spectra to the rest frame using radial velocities derived from LASP, then manually inspected for anomalous spectra and corrected their radial velocities using an empirical template spectrum. Next, we trimmed the spectra to the range 8450–8700 Å to focus on the CaT lines, and masked the major absorption features following the approach in A. Viswanathan et al. (2024). We then fitted a cubic polynomial model to the unmasked regions of the spectra, using the `curvefit` function from the `SciPy` module in `Python`.

After continuum normalization, we modeled the CaT lines separately using Gaussian profiles. We performed the fitting using the `LevMarLSQFitter` function from the `Astropy` module in `Python`. Constraints were applied to each line to ensure that the fitting parameters were reasonable. We selected 1164 VMP stars with high SNR to validate this fitting method. The left panel of Figure 2 shows that the EWs derived using Gaussian fitting agree well with direct integration results, while Figure 3 demonstrates that the fitted CaT lines match well with the normalized spectra for the example stars. In cases where the SNR was too low for Gaussian fitting, we directly integrated the spectra within 10, 15, and 12.5 Å around the line cores of the CaT lines to estimate their EWs.

We defined the CaT index (ΣCa) as the unweighted sum of the three lines $W_{8500} + W_{8544} + W_{8664}$. When the weakest CaT line W_{8500} was buried in the noise, we defined the CaT index as 1.24 times the sum of the other two lines, $1.24 \times (W_{8544} + W_{8664})$. We classified the CaT indices using two distinct flags: the CaT indices measured with all three CaT lines were assigned `flag=0`, while those measured with the two redder lines received `flag=1`. The right panel of Figure 2 demonstrates that these two definitions are consistent for VMP stars. The CaT indices were then converted to metallicities using Equation (1).

3.2. Method 2: The Color and Surface Gravity Method

Since Method 1 requires absolute magnitudes as input, it heavily relies on accurate distances. However, the geometric distances from C. A. L. Bailer-Jones et al. (2021) have significant systematic errors for stars beyond 6 kpc. In order to discover more distant VMP stars, we adopted a new method (hereafter referred to as Method 2), using the Gaia BP − RP color and surface gravity log g instead of absolute magnitude to measure metallicity. In Figure 4, we adopted a sample with surface gravity values estimated by LASP and metallicities estimated by Method 1 to show that metallicity has a good relationship with the CaT index, color, and surface gravity.

We refined the calibration from R. Carrera et al. (2013) by replacing the three terms involving magnitudes with one term for color and another term for surface gravity, as shown in Equation (2). The coefficients in this equation are shown in the

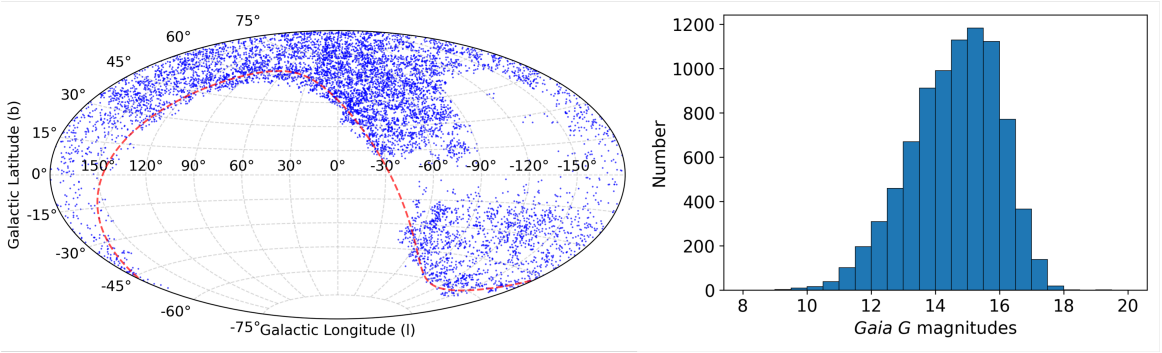

Figure 6. Left: distribution of the VMP sample in Galactic coordinates. The red-dashed line represents the celestial equator. This VMP sample covers a large area of the sky in the Northern Hemisphere. Right: distribution of the magnitudes of the VMP sample. More than 7000 stars in this VMP catalog are brighter than G 16.

right column of Table 1.

$$[\mathrm{Fe/H}] = a + b \times (G_{\mathrm{BP}} - G_{\mathrm{RP}}) + c \times \Sigma\mathrm{Ca} + d \times \log g. \quad (2)$$

The coefficients in Equation (2) were determined using a Markov Chain Monte Carlo (MCMC) procedure based on a metal-poor sample with metallicities estimated by Method 1 and surface gravity values estimated by LASP. This sample allows us to minimize the systematic errors between the two methods. Figure 5 exhibits good MCMC-fitting results, indicating that the coefficients are reliable.

Since we no longer have accurate distances for distant stars, we replaced the absolute magnitude cut with a surface gravity cut of $\log g < 3.8$, while retaining the color cut of $0.4 < G_{\mathrm{BP}} - G_{\mathrm{RP}} < 1.6$ to select MSTO and red giant stars. We use the two-dimensional dust map from E. F. Schlafly & D. P. Finkbeiner (2011) for dereddening the Gaia BP − RP color. This dust map is generally consistent with the dust map from G. M. Green et al. (2019). We removed stars with $[\mathrm{Fe/H}] > -1.5$ from the LAMOST stellar parameter catalog, as they are unlikely to be VMP stars. The final sample comprises approximately 20,000 MSTO and red giant stars with $[\mathrm{Fe/H}] < -1.5$, other than those in the the sample from Method 1. We used the same procedure as Method 1 for radial velocity correction, continuum normalization, spectral fitting, and CaT index measurements.

4. Results and Validation

We have used the methods described above to estimate the metallicities of 220,000 MSTO and red giant stars in LAMOST DR10, including 8440 VMP stars. Among these stars, 4500 metallicity estimates were obtained using Method 1, and 3940 estimates were obtained using Method 2. Figure 6 shows that this catalog covers a large area of the sky in the Northern Hemisphere, with metallicities ranging from $[\mathrm{Fe/H}] = -2.0$ to -4.0, including 25 extremely metal-poor (EMP; $[\mathrm{Fe/H}] \leqslant -3.0$) stars. More than 7000 stars are brighter than G 16, making them excellent targets for high-resolution spectroscopic follow-up with 4–10 m class telescopes.

We have validated our metallicity estimates by comparing them with the Gaia RVS metallicity catalog (A. Viswanathan et al. 2024), spectroscopic surveys such as APOGEE DR17 (S. R. Majewski et al. 2017) and GALAH DR3 (G. M. De Silva et al. 2015), high-resolution spectroscopic databases such as PASTEL (C. Soubiran et al. 2016) and SAGA (T. Suda et al. 2008), metal-poor samples from previous works such as H. Li et al. (2022), and metallicity catalogs derived using the data-driven Payne (DD-Payne) method (M. Xiang et al. 2019) and a neural network method (C. Wang et al. 2022). We only included samples with $[\mathrm{Fe/H}] < -1.5$ for comparison because the calibration used in this work is only suitable for VMP stars, and our metallicity estimates have relatively large systematic errors when compared to literature values for samples with $[\mathrm{Fe/H}] > -1.5$.

4.1. Comparison with Metal-poor Samples from Gaia RVS Spectroscopy

Figure 7 shows the validation of the metallicities estimated by Method 1. The metal-poor samples from Gaia RVS spectroscopy (A. Viswanathan et al. 2024) used the same calibration as in this work, providing an opportunity to validate our spectral analysis pipeline without introducing systematic errors from the calibration. In addition to comparing metallicities, we also compared the CaT EWs measured in both works.

From inspection of the top row of Figure 7, one can see that the metallicity estimates exhibit a negligible median offset of less than +0.01 dex, and a standard deviation of 0.13 dex, while the CaT indices show a moderate median offset of −0.11 dex, and a standard deviation of 0.25 dex. This demonstrates the robustness of our spectral analysis pipeline.

Figure 8 shows the validation of the metallicities estimated by Method 2. In the top-left panel we compared the metallicities estimated by Method 1 and Method 2, while in the top-right panel we compared the metallicities estimated by Method 2 and Gaia RVS spectroscopy (A. Viswanathan et al. 2024). Both comparisons exhibit very small median offsets of +0.01 and −0.01 dex, and moderate standard deviations of 0.15 and 0.18 dex, indicating that the calibration based on color and surface gravity is a good alternative to the calibration provided by R. Carrera et al. (2013).

4.2. Comparison with Metal-poor Samples from Spectroscopic Surveys

Next, we validated our metallicities by comparing them with metal-poor samples from spectroscopic surveys such as APOGEE DR17 (S. R. Majewski et al. 2017) and GALAH DR3 (G. M. De Silva et al. 2015). We removed stars with `FE_H_FLAG≠0` from the APOGEE sample and stars with `flag_fe_h≠0` from the GALAH sample.

From inspection of the second row of Figure 7, one can see that the metallicities estimated by Method 1 exhibit a tiny median

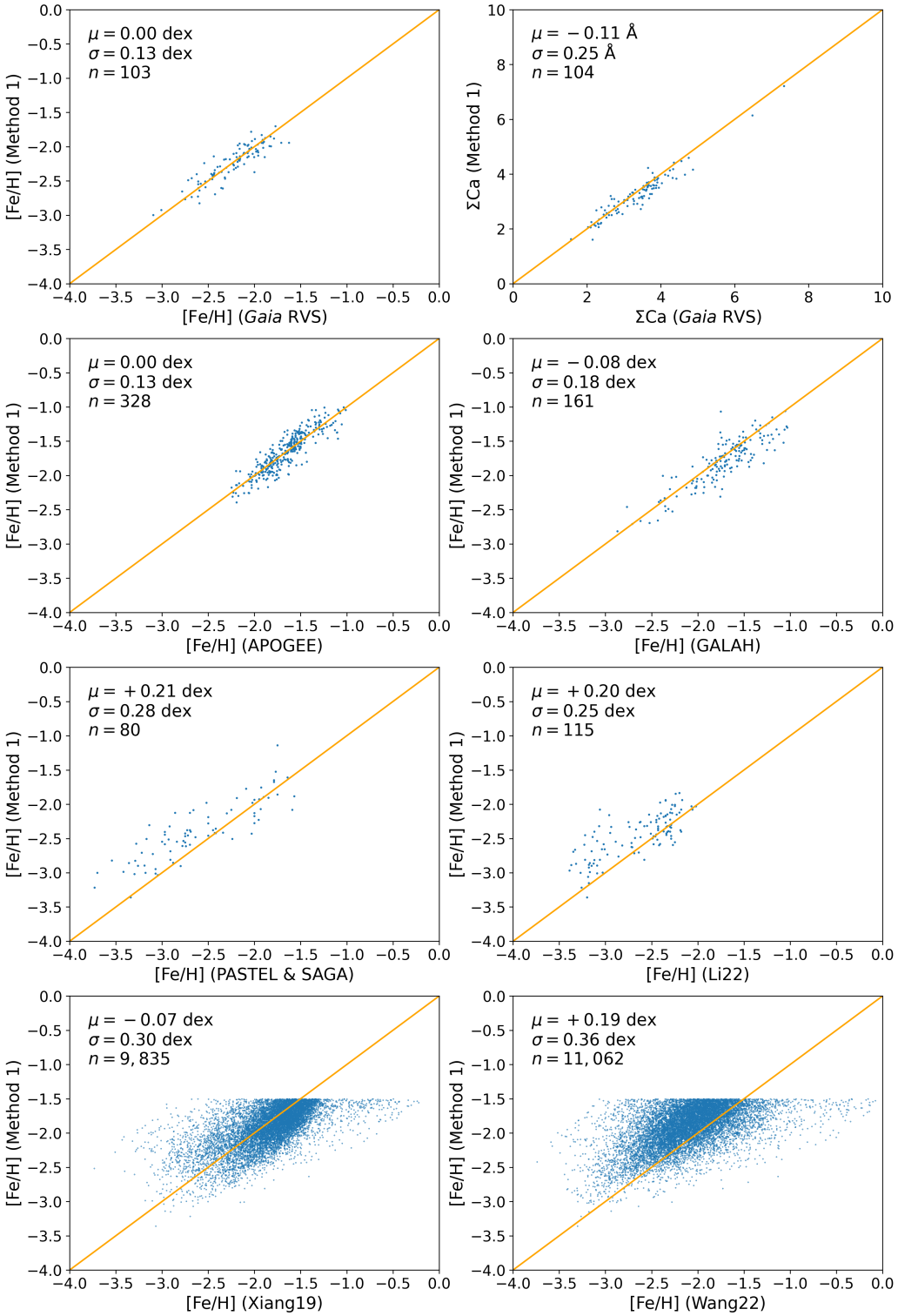

Figure 7. Top row: comparison of metallicities (left) and CaT EWs (right) estimated by Method 1 with results from Gaia RVS spectroscopy. Second row: comparison with spectroscopic surveys such as APOGEE DR17 (left) and GALAH DR3 (right). Third row: comparison with metal-poor samples from high-resolution spectroscopy such as PASTEL and SAGA (left) and H. Li et al. (2022) (right). Bottom row: comparison with metallicity catalogs from M. Xiang et al. (2019) (left) and C. Wang et al. (2022) (right). The number of matches (n), median offset (μ), and standard deviation (σ) of [Fe/H] and ΣCa are shown at the top of each panel. The orange lines represent the 1:1 line.

offset of less than +0.01 dex, and a moderate standard deviation of 0.13 dex when compared to the APOGEE sample, while showing a slightly larger, but still very small, median offset of −0.08 dex, and a moderate standard deviation of 0.18 dex when compared to the GALAH sample. This indicates that our metallicity estimates are reliable for VMP stars.

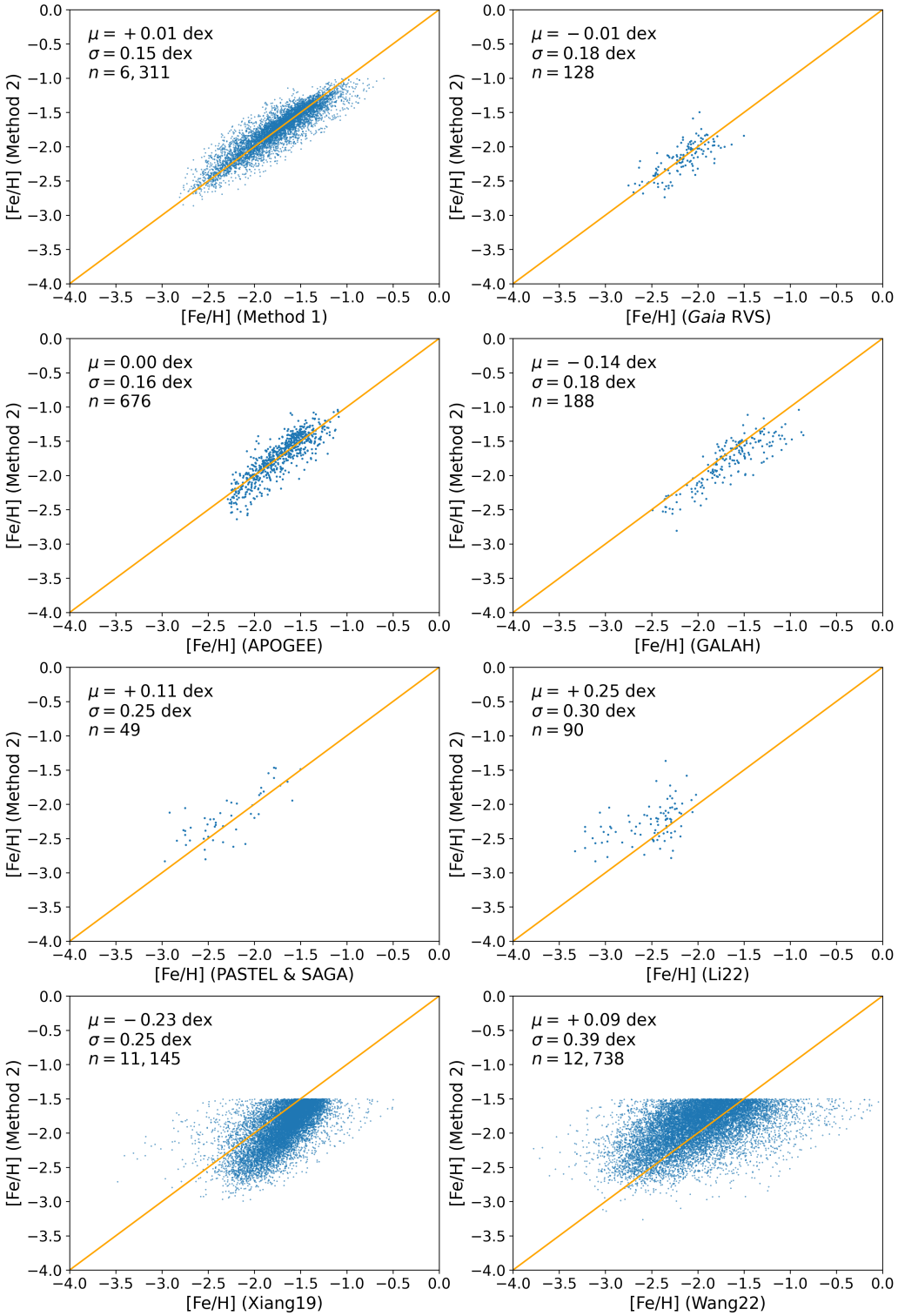

Figure 8. Top row: comparison between metallicities estimated by Method 1 and Method 2 (left) and comparison between metal-poor samples from Method 2 and Gaia RVS spectroscopy (right). Second row: comparison with spectroscopic surveys such as APOGEE DR17 (left) and GALAH DR3 (right). Third row: comparison with metal-poor samples from high-resolution spectroscopy such as PASTEL and SAGA (left) and H. Li et al. (2022) (right). Bottom row: comparison with metallicity catalogs from M. Xiang et al. (2019) (left) and C. Wang et al. (2022) (right). The number of matches (n), median offset (μ), and standard deviation (σ) of [Fe/H] are shown at the top of each panel. The orange lines represent the 1:1 line.

The second row of Figure 8 shows that the metallicities estimated by Method 2 exhibit a tiny median offset of less than +0.01 dex, and a moderate standard deviation of 0.16 dex when compared to the APOGEE sample, while showing a larger median offset of −0.14 dex, and a moderate standard deviation of 0.18 dex when compared to the GALAH sample.

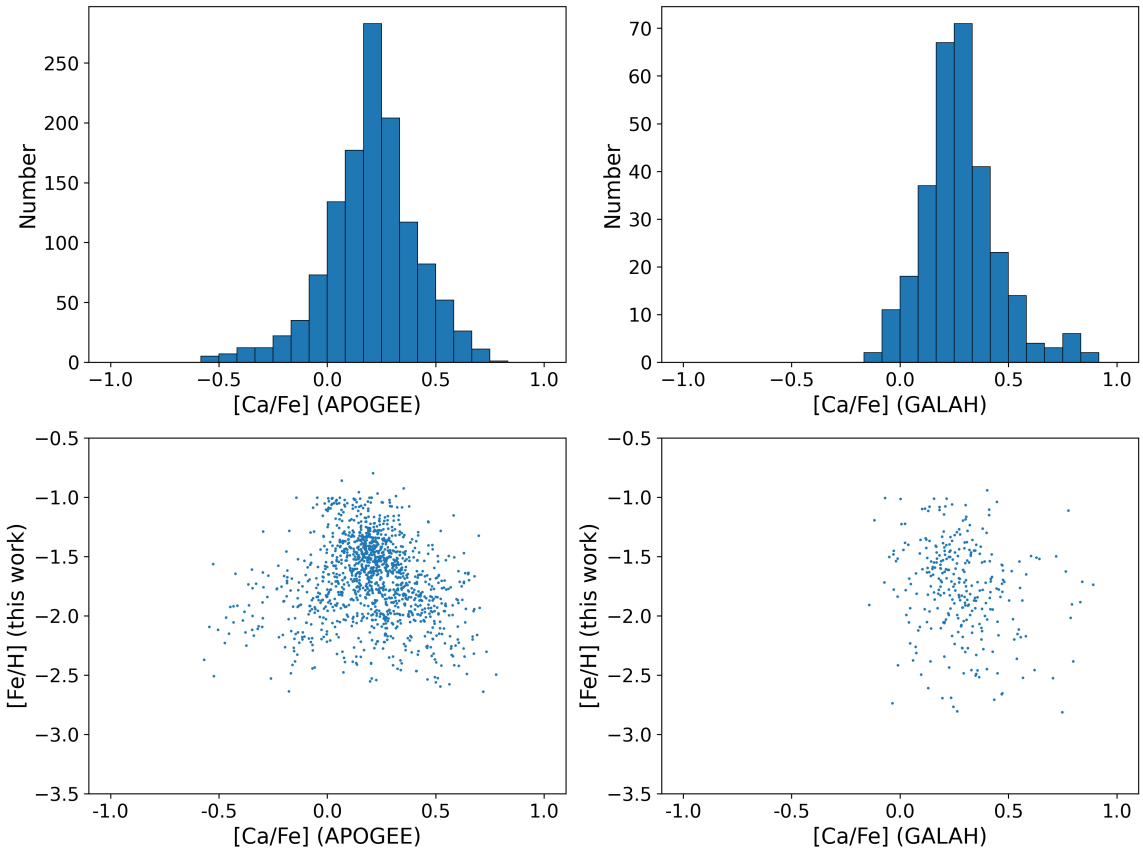

Figure 9. Top row: the [Ca/Fe] distribution of metal-poor stars in this work using measurements from APOGEE (left) and GALAH (right). Bottom row: the distribution of [Fe/H] measured in this work vs. the [Ca/Fe] measured by APOGEE (left) and GALAH (right).

Generally, the comparison of metallicities estimated by Method 1 and Method 2 have similar trends, probably because the coefficients of the calibration used in Method 2 were derived with a sample from Method 1, and thus Method 2 inherited the systematic offsets from Method 1.

We also validated the calcium abundance for the metal-poor stars in this work using [Ca/Fe] from APOGEE and GALAH. The top row of Figure 9 demonstrates that the [Ca/Fe] of most metal-poor stars are between 0.0 and +0.4, while the bottom row of Figure 9 shows no significant correlation between the [Ca/Fe] and [Fe/H] of these stars. Given this relatively narrow spread and lack of strong correlation, we do not apply any explicit correction for calcium abundance in our [Fe/H] calibration based on CaT lines. However, we adopt a conservative empirical uncertainty of 0.2 dex to account for possible variations due to [Ca/Fe].

4.3. Comparison with Metal-poor Samples from High-resolution Spectroscopy

To validate our metallicities in the EMP regime, we compared them with metal-poor samples from high-resolution spectroscopic databases such as PASTEL (C. Soubiran et al. 2016) and SAGA (T. Suda et al. 2008), as well as results from previous works based on high-resolution spectroscopy, such as H. Li et al. (2022).

Inspection of the third row of Figure 7 shows that the metallicity estimates in this work exhibit moderate median offsets of +0.21 and +0.20 dex, and standard deviations of 0.28 and 0.25 dex when compared to high-resolution results. The metallicities estimated by Method 1 are higher in the EMP regime than in the VMP regime, because the calibration used in Method 1 saturates in the EMP regime (R. Carrera et al. 2013).

The third row of Figure 8 also exhibits moderate median offsets of +0.11 and +0.25 dex, and standard deviations of 0.25 and 0.30 dex. This comparison lacks EMP stars because we used surface gravity values estimated by LASP, which did not assign stellar parameters to EMP stars. However, we will be able to identify EMP stars using this method once we will have access to additional sources of surface gravity data in the future.

4.4. Comparison with Metallicities Estimated by DD-Payne and Neural Network Methods

The bottom row of Figure 7 shows comparisons with metal-poor samples from M. Xiang et al. (2019) using the DD-Payne method, and metal-poor samples from C. Wang et al. (2022) using a neural network method. The DD-Payne model was trained with samples from GALAH DR2 (S. Buder et al. 2018) and APOGEE DR14 (J. A. Holtzman et al. 2018), while the neural network model was trained with samples from PASTEL (C. Soubiran et al. 2016).

The bottom row of Figure 7 exhibits a very small median offset of −0.07 dex and a standard deviation of 0.30 dex compared to M. Xiang et al. (2019), and a moderate median offset of +0.19 dex and a standard deviation of 0.36 dex compared to C. Wang et al. (2022). The bottom row of Figure 8 exhibits similar results, with a larger median offset of

Table 2
Description of the Columns in the Metallicity Catalog in this Work

Column	Description	Unit
obsid	LAMOST DR10 unique spectrum ID	…
gaiaid	Gaia DR3 source ID	…
ra	Gaia DR3 R.A. in ICRS (J2016) format	degrees
dec	Gaia DR3 decl. in ICRS (J2016) format	degrees
snr	Signal-to-noise ratio at the r band of the LAMOST spectrum	…
g_mag	Gaia G magnitude	mag
g_err	Uncertainty of the Gaia G magnitude	mag
bp_mag	Gaia $G_{\rm BP}$ magnitude	mag
bp_err	Uncertainty of the Gaia $G_{\rm BP}$ magnitude	mag
rp_mag	Gaia $G_{\rm RP}$ magnitude	mag
rp_err	Uncertainty of the Gaia $G_{\rm RP}$ magnitude	mag
teff_LASP	Effective temperature estimated by A. L. Luo et al. (2015)	K
teff_err_LASP	Uncertainty of the effective temperature estimated by A. L. Luo et al. (2015)	K
logg_LASP	Surface gravity estimated by A. L. Luo et al. (2015)	cgs
logg_err_LASP	Uncertainty of the surface gravity estimated by A. L. Luo et al. (2015)	cgs
feh_LASP	Metallicity estimated by A. L. Luo et al. (2015)	…
feh_err_LASP	Uncertainty of the metallicity estimated by A. L. Luo et al. (2015)	dex
pm	Gaia DR3 proper motion	mas yr^{-1}
pmra	Gaia DR3 proper motion in R.A.	mas yr^{-1}
pmra_err	Uncertainty of the Gaia DR3 proper motion in R.A.	mas yr^{-1}
pmdec	Gaia DR3 proper motion in decl.	mas yr^{-1}
pmdec_err	Uncertainty of the Gaia DR3 proper motion in decl.	mas yr^{-1}
rv	Radial velocity offset from the rest frame	km s^{-1}
rv_err	Uncertainty of the radial velocity offset from the rest frame	km s^{-1}
rgeo	Geometric distance estimated by C. A. L. Bailer-Jones et al. (2021)	pc
rgeo_err	Uncertainty of the geometric distance estimated by C. A. L. Bailer-Jones et al. (2021)	pc
ebv	Interstellar reddening	mag
g_corr	Dereddened Gaia G magnitude	mag
bp_corr	Dereddened Gaia $G_{\rm BP}$ magnitude	mag
rp_corr	Dereddened Gaia $G_{\rm RP}$ magnitude	mag
ew1	Equivalent width of the first calcium triplet line at 8500 Å	Å
err1	Uncertainty of the equivalent width of the first calcium triplet line at 8500 Å	Å
chi1	The χ^2 of the spectra fitting of the first calcium triplet line at 8500 Å	…
ew2	Equivalent width of the second calcium triplet line at 8544 Å	Å
err2	Uncertainty of the equivalent width of the second calcium triplet line at 8544 Å	Å
chi2	The χ^2 of the spectra fitting of the second calcium triplet line at 8544 Å	…
ew3	Equivalent width of the third calcium triplet line at 8664 Å	Å
err3	Uncertainty of the equivalent width of the third calcium triplet line at 8664 Å	Å
chi3	The χ^2 of the spectra fitting of the third calcium triplet line at 8664 Å	…
err	The average noise of the continuum in the spectrum	Å
flag	Quality flag of the equivalent width of the first calcium triplet line at 8500 Å	…
feh	Spectroscopic metallicity derived in this work using LAMOST spectrum	…
feh_err	Uncertainty of the spectroscopic metallicity derived in this work	dex
method	Method used in deriving spectroscopic metallicity	…

(This table is available in its entirety in machine-readable form in the online article.)

-0.23 dex and a standard deviation of 0.25 dex compared to M. Xiang et al. (2019), and a smaller median offset of $+0.09$ dex and a standard deviation of 0.39 dex compared to C. Wang et al. (2022).

The bottom row of this figure shows greater dispersions than the upper rows, probably due to the combined errors from both our sample and the sample from M. Xiang et al. (2019) and C. Wang et al. (2022). The systematic offset in the bottom-left panel occurs because the DD-Payne model saturates at $[{\rm Fe/H}] < -2.5$, while the offset in the bottom-right panel arises from the difference between low-resolution spectra from LAMOST and the high-resolution spectra from PASTEL. Overall, the metallicities estimated in this work agree with the results from M. Xiang et al. (2019) and C. Wang et al. (2022).

5. Summary

The search for VMP stars has long been a challenging yet central pursuit in Galactic archeology. In the past decade, data mining of photometric and spectroscopic surveys has led to numerous successful discoveries of VMP stars in the Galaxy. LAMOST DR10 has released over 12 million spectra for stars in the Milky Way, providing a great opportunity for discovering VMP stars. Unlike previous studies, we focus on the red arm of LAMOST spectra because its high SNR enables the analysis of a larger sample size and more accurate metallicity estimates. We derived metallicities using the EWs of the CaT lines in the near-infrared band of LAMOST low-resolution spectra, applying an empirical calibration from R. Carrera et al. (2013). Additionally, we refined this

calibration by replacing absolute magnitude with Gaia BP − RP color and LAMOST surface gravity, facilitating the discovery of distant VMP stars without the need for accurate distance measurements.

In this work, we present a metallicity catalog of 8440 VMP MSTO and red giant stars based on low-resolution spectra from LAMOST DR10. The primary parameters of the catalog are listed in Table 2. This catalog covers a large area of sky in the Northern Hemisphere, with metallicities ranging from [Fe/H] = −2.0 to −4.0. In addition to metallicities, we also provide distances, proper motions, and radial velocities from which complete six-dimensional dynamic data can be derived for the sample stars. About 4000 stars are located farther than 6 kpc, and more than 7000 stars are brighter than G 16. These bright VMP stars are excellent targets for high-resolution spectroscopic follow-up with 4–10 m class telescopes. Validity checks through comparisons with metal-poor samples from spectroscopic surveys and high-resolution spectroscopy demonstrate that the metallicity estimates in this work are robust and reliable, with an average median offset of 0.1 dex and an average standard deviation of 0.2 dex.

The ongoing data releases from the Gaia project will provide accurate parallaxes and proper motions for billions of stars in the Milky Way, which are expected to significantly improve the accuracy of stellar parameters, especially surface gravity. Moreover, future data releases from spectroscopic surveys such as LAMOST DR12 and DESI DR1 will provide spectra for millions of stars in the Galaxy. The combination of future surveys will result in an unprecedented multiparameter catalog of Galactic stars, offering an enormous opportunity to explore the nature of the early Milky Way.

Acknowledgments

Y.H. acknowledges support by the National Natural Science Foundation of China grant No. 12422303, the National Key R&D Program of China No. 2023YFA1608303, and the Fundamental Research Funds for the Central Universities (grant Nos. 118900M122, E5EQ3301X2, and E4EQ3301X2). H.W.Z. acknowledges support by the National Key R&D Program of China No. 2024YFA1611903. T.C.B. acknowledges partial support for this work from grant PHY 14-30152; Physics Frontier Center/JINA Center for the Evolution of the Elements (JINA-CEE), and OISE-1927130: The International Research Network for Nuclear Astrophysics (IReNA), awarded by the US National Science Foundation. Guoshoujing Telescope (the Large sky Area Multi-Object Fiber Spectroscopic Telescope, LAMOST) is a National Major Scientific Project built by the Chinese Academy of Sciences. Funding for the project has been provided by the National Development and Reform Commission. LAMOST is operated and managed by the National Astronomical Observatories, Chinese Academy of Sciences.

Software: NumPy (C. R. Harris et al. 2020), Matplotlib (J. D. Hunter 2007), SciPy (P. Virtanen et al. 2020), Astropy (Astropy Collaboration et al. 2022), TOPCAT (M. B. Taylor 2005).

ORCID iDs

Huiling Chen https://orcid.org/0009-0008-2988-2680
Yang Huang https://orcid.org/0000-0003-3250-2876
Huawei Zhang https://orcid.org/0000-0002-7727-1699
Timothy C. Beers https://orcid.org/0000-0003-4573-6233

References

Astropy Collaboration, Price-Whelan, A. M., Lim, P. L., et al. 2022, ApJ, 935, 167
Bailer-Jones, C. A. L., Rybizki, J., Fouesneau, M., Demleitner, M., & Andrae, R. 2021, AJ, 161, 147
Beers, T. C., & Christlieb, N. 2005, ARA&A, 43, 531
Beers, T. C., Preston, G. W., & Shectman, S. A. 1985, AJ, 90, 2089
Beers, T. C., Preston, G. W., & Shectman, S. A. 1992, AJ, 103, 1987
Buder, S., Asplund, M., Duong, L., et al. 2018, MNRAS, 478, 4513
Cabrera Garcia, J., Beers, T. C., Huang, Y., et al. 2024, MNRAS, 527, 8973
Carrera, R., Pancino, E., Gallart, C., & del Pino, A. 2013, MNRAS, 434, 1681
Cenarro, A. J., Moles, M., Cristóbal-Hornillos, D., et al. 2019, A&A, 622, A176
Christlieb, N., Schörck, T., Frebel, A., et al. 2008, A&A, 484, 721
Cui, X.-Q., Zhao, Y.-H., Chu, Y.-Q., et al. 2012, RAA, 12, 1197
De Silva, G. M., Freeman, K. C., Bland-Hawthorn, J., et al. 2015, MNRAS, 449, 2604
Fan, Z., Zhao, G., Wang, W., et al. 2023, ApJS, 268, 9
Gaia Collaboration, Vallenari, A., Brown, A. G. A., et al. 2023, A&A, 674, A1
Green, G. M., Schlafly, E., Zucker, C., Speagle, J. S., & Finkbeiner, D. 2019, ApJ, 887, 93
Harris, C. R., Millman, K. J., van der Walt, S. J., et al. 2020, Natur, 585, 357
Holtzman, J. A., Hasselquist, S., Shetrone, M., et al. 2018, AJ, 156, 125
Hong, J., Beers, T. C., Lee, Y. S., et al. 2024, ApJS, 273, 12
Huang, Y., Beers, T. C., Wolf, C., et al. 2022, ApJ, 925, 164
Huang, Y., Beers, T. C., Xiao, K., et al. 2024, ApJ, 974, 192
Huang, Y., Beers, T. C., Yuan, H., et al. 2023, ApJ, 957, 65
Huang, Y., Chen, B. Q., Yuan, H. B., et al. 2019, ApJS, 243, 7
Hunter, J. D. 2007, CSE, 9, 90
Ishigaki, M. N., Tominaga, N., Kobayashi, C., & Nomoto, K. 2018, ApJ, 857, 46
Klessen, R. S., & Glover, S. C. O. 2023, ARA&A, 61, 65
Li, H., Aoki, W., Matsuno, T., et al. 2022, ApJ, 931, 147
Li, H., Tan, K., & Zhao, G. 2018, ApJS, 238, 16
Luo, A. L., Zhao, Y.-H., Zhao, G., et al. 2015, RAA, 15, 1095
Majewski, S. R., Schiavon, R. P., Frinchaboy, P. M., et al. 2017, AJ, 154, 94
Mendes de Oliveira, C., Ribeiro, T., Schoenell, W., et al. 2019, MNRAS, 489, 241
Riello, M., De Angeli, F., Evans, D. W., et al. 2021, A&A, 649, A3
Rockosi, C. M., Lee, Y. S., Morrison, H. L., et al. 2022, ApJS, 259, 60
Schlafly, E. F., & Finkbeiner, D. P. 2011, ApJ, 737, 103
Shank, D., Beers, T. C., Placco, V. M., et al. 2022, ApJ, 926, 26
Shank, D., Beers, T. C., Placco, V. M., et al. 2023, ApJ, 943, 23
Soubiran, C., Le Campion, J.-F., Brouillet, N., & Chemin, L. 2016, A&A, 591, A118
Starkenburg, E., Martin, N., Youakim, K., et al. 2017, MNRAS, 471, 2587
Steinmetz, M., Zwitter, T., Siebert, A., et al. 2006, AJ, 132, 1645
Suda, T., Katsuta, Y., Yamada, S., et al. 2008, PASJ, 60, 1159
Taylor, M. B. 2005, in ASP Conf. Ser. 347, Astronomical Data Analysis Software and Systems XIV, ed. P. Shopbell, M. Britton, & R. Ebert (San Francisco, CA: ASP), 29
Virtanen, P., Gommers, R., Oliphant, T. E., et al. 2020, NatMe, 17, 261
Viswanathan, A., Starkenburg, E., Matsuno, T., et al. 2024, A&A, 683, L11
Wang, C., Huang, Y., Yuan, H., et al. 2022, ApJS, 259, 51
Wolf, C., Onken, C. A., Luvaul, L. C., et al. 2018, PASA, 35, e010
Xiang, M., Ting, Y.-S., Rix, H.-W., et al. 2019, ApJS, 245, 34
Yanny, B., Rockosi, C., Newberg, H. J., et al. 2009, AJ, 137, 4377
Zepeda, J., Beers, T. C., Placco, V. M., et al. 2023, ApJ, 947, 23
Zhao, G., Zhao, Y.-H., Chu, Y.-Q., Jing, Y.-P., & Deng, L.-C. 2012, RAA, 12, 723